Oxygen incorporation into strontium titanate single crystals from CO_2 dissociation

Chr. Argirusis,*[ab] F. Voigts,[c] P. Datta,[a] J. Grosse-Brauckmann[a] and W. Maus-Friedrichs[c]

Received 22nd January 2009, Accepted 17th March 2009
First published as an Advance Article on the web 26th March 2009
DOI: 10.1039/b901401b

Oxygen incorporation from CO_2 into Fe-doped $SrTiO_3$(100) single crystals (0.013 at% Fe, 0.039 at% Fe and 0.13 at% Fe) was investigated. Oxygen incorporation processes using $^{13}C^{18}O_2$ as the gas source were studied by isotope exchange depth profiling (IEDP) and subsequent secondary-ion mass spectroscopy (SIMS). The interaction of CO_2 with $SrTiO_3$ (100) surfaces was further studied with different surface analytical techniques like metastable induced electron spectroscopy (MIES), ultraviolet photoelectron spectroscopy (UPS) and X-ray photoelectron spectroscopy (XPS). Results indicate that CO_2 interaction with $SrTiO_3$ (100) surfaces does not change the surface at all. It seems that CO_2 provides a very low sticking probability on the surface as it is not traced by valence band spectroscopy even at room temperature. Nonetheless, $^{13}C^{18}O_2$ acts as an incorporation source of ^{18}O into the Fe-doped $SrTiO_3$ single crystals. The diffusion coefficient exhibits a peculiar behaviour when Fe concentration increases. No carbon incorporation is observed at all.

1. Introduction

$SrTiO_3$ is a model oxide for electroceramics. It is a typical ABO_3-type perovskite material with remarkable thermal and chemical stability and easy fabricability. As a result, $SrTiO_3$ has found applications in a wide range of technologically relevant fields like capacitors, oxygen sensors, dielectrics as well as substrates for superconducting materials. Moreover, depending on the conditions it can show ionic conduction or p- or n-type electronic conduction. The key point that enables one to render this material with a specific conductivity is its suitability to dope this material with aliovalent dopants without changing its crystal structure.[1,2] $SrTiO_3$ is stable and shows no phase transitions between −170 °C and 2570 °C.[3] It is not surprising that this technologically important material has caught the attention of researchers and a plethora of research activity is going on to understand various issues of this material.[4–9] Defect chemical basics of this material can be found in the literature[10–12] and in the references therein. Recently Merkle and Maier[13] discussed the oxygen incorporation in oxides on the example of $SrTiO_3$ as a model material.

One important use of $SrTiO_3$ is its application as resistive high-temperature oxygen sensor,[14,15] with the analysis of combustion engine exhaust being one important utilisation. The effect is based on the equilibrium between bulk oxygen defects and the surrounding oxygen partial pressure. At high pressures, oxygen molecules are dissociated in front of the surface and the oxygen atoms are incorporated into the bulk, and *vice versa* for low pressures. The oxygen vacancy density determines the macroscopic conductivity of the crystal and can be measured electrically. As the diffusion of oxygen vacancies is quite fast at temperatures above 700 °C,[16] the dissociation processes are the rate-limiting step for this reaction. This means optimizing the surface density of states (SDOS) of the $SrTiO_3$ with respect to the dissociation probability may be very important to achieve quick response times from a $SrTiO_3$ oxygen sensor. Hence, the $SrTiO_3$ surface is being studied intensively with surface analytical methods like metastable induced electron spectroscopy (MIES), ultraviolet photoelectron spectroscopy (UPS) and X-ray photoelectron spectroscopy (XPS).

The cross-sensitivity of the sensor to other oxygen sources present in exhaust like CO, CO_2 or H_2O is of great importance for any practical use and depends on the interaction of the above mentioned molecules with the surface. The sensor response behaviour obviously depends on the oxygen exchange kinetics. The basic oxygen incorporation reaction can be written as (Kröger–Vink notation):

$$\tfrac{1}{2}O_2(g) + V_O^{\bullet\bullet} \Leftrightarrow O_O^x + 2h^{\bullet} \quad (1)$$

This reaction is a three step process: dissociation of the oxygen molecule in the vicinity of the surface, the oxygen surface transfer which includes all surface-related electrochemical processes and the subsequent chemical diffusion of oxygen. The response behaviour of the sensor is determined by the slowest step which determines the kinetics of the overall process.

The most convenient way of studying oxygen incorporation in a crystalline solid is by the means of tracer isotope

[a] *School of Chemical Engineering, National Technical University of Athens, Iroon Polytechneiou 9, Zografou 157 80, Athens, Greece*
[b] *Institut für Metallurgie, Technische Universität Clausthal, Robert-Koch-Str. 42, 38678 Clausthal-Zellerfeld, Germany. E-mail: christos.argirusis@tu-clausthal.de; Fax: +30 (0)210 772 3244; Tel: +30 (0)210 772 2254*
[c] *Institut für Physik und Physikalische Technologien, Technische Universität Clausthal, Leibnizstrasse 4, 38678 Clausthal-Zellerfeld, Germany*

exchange. In this process the oxygen incorporation consists of a surface reaction at the gas/solid interface which is characterized by the surface-exchange rate constant and a subsequent bulk transport which is characterized by the diffusion coefficient. The objective of this investigation is to see whether different gaseous contaminants influence oxygen incorporation reaction in acceptor-doped $SrTiO_3$. Results for oxygen incorporation from CO_2 sources are reported.

2. Experimental

Single crystals of $SrTiO_3$(100) were supplied by CrysTec GmbH (Berlin, Germany). First, each of the three differently doped $SrTiO_3$ single crystals (0.13, 0.039 and 0.013 at% Fe corresponding to 1.1×10^{20}, 3.3×10^{19} and 1.1×10^{19} Fe atoms per cm^3) were cut from one boule each with dimensions of $5 \times 5 \times 1$ mm and crystals were polished down to optical finish with the dimension 0.1 μm. These three types of samples will be henceforth referred to as LC-STO ("low content" with low dopant content of the $SrTiO_3$), MC-STO ("medium content") and HC-STO ("high content" for highly doped $SrTiO_3$).

For the diffusion experiments, all samples were first heated at 1000 °C for 24 h in 200 mbar of $^{16}O_2$ in order to remove any remnants from the polishing process and to equilibrate the balance of defects at the surface. The samples were equilibrated at any temperature for about ten times the estimated subsequent diffusion time in an oxygen partial pressure similar to the subsequent diffusion. Three sets of samples were then annealed separately in $^{13}C^{18}O_2$ (99% ^{13}C and 95% ^{18}O, Campro Scientific, Berlin, Germany) at various temperatures starting from 850 to 1000 °C for an annealing time of 6 to 16 h. In all cases the partial pressure of $^{13}C^{18}O_2$ was kept fixed at 200 mbar. Before letting in the gas into the annealing chamber, it was evacuated to the tune of 10^{-5} mbar using a turbomolecular pump. The ^{18}O concentration profiles of the exposed samples were analyzed by means of secondary-ion mass spectroscopy (SIMS) using a Cameca 4f with a Cs^+ ion source (primary ion energy 10 kV). As the diffusivity of oxygen in Fe-doped $SrTiO_3$ is high in the examined temperature regime, the tracer depth profile is beyond the measuring limit of SIMS. So, the line scan technique was adopted. The line scan mode is always used when the diffusion takes place very quickly resulting in diffusion depths much longer than the typical surface depth profiles of 1 μm. Typical diffusion depths in the line scan mode are about 50–300 μm. For SIMS investigations in the line scan mode the exchanged samples were cut perpendicular to the exposed surface, and polished and coated with gold before measurement in order to prevent charging during SIMS measurement. The line scan was performed with a step of 1 μm.

^{18}O depth profiles could be evaluated by the solution of the diffusion equation in a semi-infinite medium which is given below:[17]

$$\frac{c(x,t)-c(t=0)}{c(t=\infty)-c(t=0)} = \operatorname{erfc}\left(\frac{x}{2\sqrt{D^*t}}\right) - \exp\left(\frac{k^*x}{D^*}+\frac{k^{*2}t}{D^*}\right)\operatorname{erfc}\left(\frac{x}{2\sqrt{D^*t}}+\frac{k^*}{D^*}\sqrt{D^*t}\right) \quad (2)$$

where D^* and k^* are tracer diffusion and tracer surface exchange coefficients and the other notations have their usual meaning. This equation can be safely used for the solution as diffusion lengths were smaller than sample half width.

An ultrahigh vacuum (UHV) apparatus with a base pressure of 5×10^{-11} mbar, details of which can be found elsewhere,[18] was used to carry out the surface spectroscopic measurements.

Electron spectroscopy was performed using a hemispherical analyzer (VSW HA100) in combination with a source for metastable helium atoms (mainly He* $^3S_1$) and ultraviolet photons (HeI line). A commercial non-monochromatic X-ray source (Specs RQ20/38C) was used for XPS.

During XPS, X-ray photons hit the surface under an angle of 80° to the surface normal, illuminating a spot of several mm in diameter. For all measurements presented here, the Al Kα line with photon energy of 1486.7 eV was used. Electrons were recorded by the hemispherical analyzer with an energy resolution of 1.1 eV under an angle of 10° to the surface normal. All XPS spectra are displayed as a function of binding energy with respect to the Fermi level.

For quantitative XPS analysis, photoelectron peak areas were calculated *via* mathematical fitting with Gauss-type profiles. Photoelectric cross sections as calculated by Scofield[19] and inelastic mean free paths from the NIST database[20] as well as the energy-dependent transmission function of the hemispherical analyzer were taken into account when calculating stoichiometry.

MIES and UPS were performed applying a cold cathode gas discharge *via* a two-stage pumping system. A time-of-flight technique was employed to separate electrons emitted by He* (MIES) from those induced by HeI (UPS) interaction with the surface. The combined He*–HeI beam strokes the sample surface under an angle of 45° to the surface normal and illuminated a spot of approximately 2 mm in diameter. The spectra were recorded simultaneously by the hemispherical analyzer with an energy resolution of 220 meV under normal emission within 150 s.

MIES is an extremely surface sensitive technique probing solely the outermost layer of the sample, because the He* atoms interact with the surface typically 0.3 to 0.5 nm in front of it. This may occur *via* a number of different mechanisms depending on surface electronic structure and work function, as has been described in detail elsewhere.[21–23] Only the processes relevant for the spectra presented here will be discussed in the following sections.

An electron from the sample fills the 1s orbital of the impinging He* during Auger deexcitation (AD). Simultaneously, the He 2s electron is emitted carrying the excess energy. The resulting spectra reflect the surface density of states (SDOS) directly. AD-MIES and UPS can be compared which allows a distinction between surface and bulk effects.

For STO, a different kind of interaction takes place: the 2s electron of the impinging He* is resonantly transferred into the surface of the sample and localizes at near surface Ti 3d states. Subsequently, a Ti 3d electron fills the hole in He^+ 1s in an interatomic Auger neutralization (AN) process, followed by the emission of an O 2p surface electron carrying the excess energy. The energy of the resulting MIES peak is shifted by 1.2 eV toward higher binding energies compared to AD due to

a diminished local ionization potential. A detailed discussion of this process is given in another report.[24]

All MIES and UPS spectra are shown as a function of the electron binding energy with respect to the Fermi level. The surface work function can be determined from the high binding energy onset of the MIES or the UPS spectra with an accuracy of ±0.1 eV.

For the UHV experiments, the $SrTiO_3$ was mounted in a sample manipulator by means of a molybdenum holder, which was fitted with a backside electron bombardment heating system for the sample. All spectroscopic experiments were performed *in situ* and at room temperature, except noted otherwise.

CO_2 (99.995%, Linde Gas) was injected *via* backfilling the chamber using a bakeable leak valve. The gas line was evacuated and heated in order to ensure cleanness. Additionally, a cold-trap was installed to minimize water contamination during gas injection. A quadrupole mass spectrometer (Balzers QMS 112A) was used to monitor the partial pressure of the residual gases simultaneously during all exposure experiments.

Additional gas-exchange experiments were performed at a second UHV apparatus with similar characteristics, which has been described in detail previously.[25] For these experiments, the sample is heated in the presence of different gases. The temperature is monitored by a type C thermocouple and the gas phase directly in front of the sample is observed with a temperature-programmed desorption (TPD) system (Balzers QMA 125) and all gases emitting from the surface are recorded.

3. Results

Based on the work of Claus *et al.*[26] meaningful diffusion times for a maximum diffusion depth of 250 μm were calculated. Based on that, tracer diffusion coefficients were extrapolated for the three Fe-doped samples assuming a linear correlation between dopant concentration and diffusivity.

The first difficulty that was encountered in determining the diffusion coefficients in the first attempts was that the differently doped samples showed diffusion coefficients which were orders of magnitude different. For the sake of comparability, all experiments should be carried out at similar experimental conditions, therefore at each temperature the samples were kept in the furnace at the same time, leading to comparable samples.

Fig. 1 to 3 show the depth profiles of the HC-STO, MC-STO and LC-STO samples, respectively. It is obvious that the differently doped samples show significantly different depth profiles. High contents samples showed reasonable diffusion depth profile and they could be measured by a normal depth profile analysis with SIMS. However, the low content samples show diffusion lengths, which are more by a factor of 30 to 60 greater under the same conditions as can be seen by comparing Fig. 1 and 3. This is the reason that the measurements were done in the "line-scan mode" for the low content samples.

The oxygen incorporates into the material at high incorporation rates, practically comparable with the ones resulting from an oxygen atmosphere.[27,28] Fig. 4 shows an Arrhenius plot of k^* and D^* values obtained by fitting the diffusion

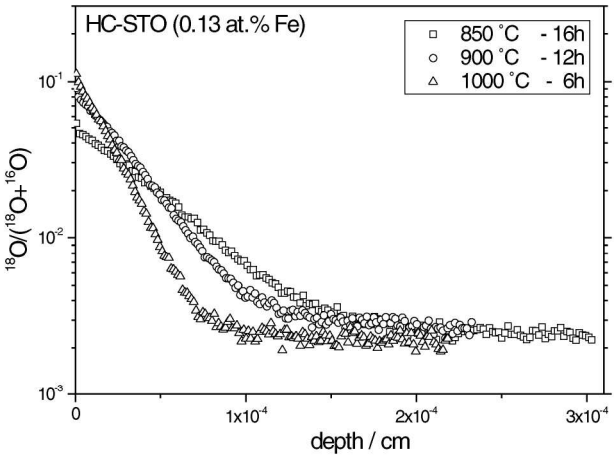

Fig. 1 ^{18}O tracer diffusion in HC-STO (0.13 at% Fe) from $^{13}C^{18}O_2$ exposure.

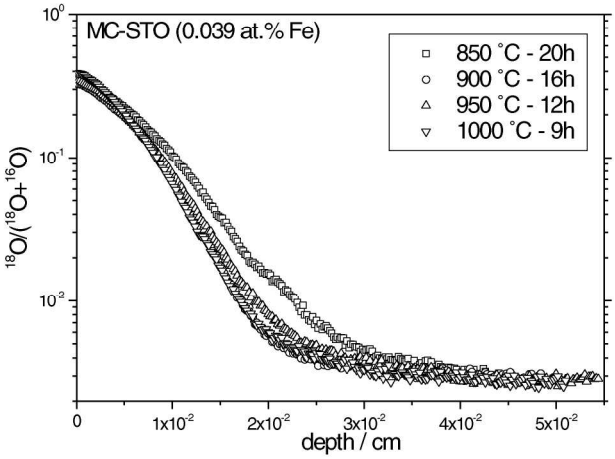

Fig. 2 ^{18}O tracer diffusion in MC-STO (0.039 at% Fe) from $^{13}C^{18}O_2$ exposure.

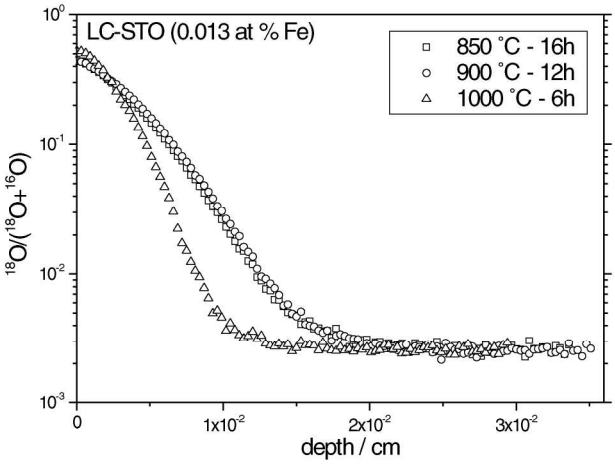

Fig. 3 ^{18}O tracer diffusion in LC-STO (0.013 at% Fe) from $^{13}C^{18}O_2$ exposure.

profiles of the investigated samples with eqn (2) along with activation energies for the k^*. It is noted that the activation energies of HC- and LC-STO are quite similar whereas that of

MC-STO is a little lower than the other two. Regarding their dependence on the dopant concentration the diffusion coefficients show a similar behaviour like the surface exchange coefficients meaning that the diffusivities are much lower for the high dopant content. While the diffusivities for the samples with lower and medium dopant content are in the same range of values reported in the literature, the diffusivities for the high content material are much lower (about 4 orders of magnitude) than literature data, where it is reported that increasing the dopant content results to higher diffusivities (in our case valid for lower and medium dopant content).[26]

Several XPS survey spectra of $SrTiO_3$ are shown in Fig. 5, which have been taken for chemical analysis. The photoelectron count rate is plotted *versus* the electron binding energy. Photoelectron peaks and Auger electron structures are denoted by the correspondent atomic orbitals and Auger energy levels, respectively. The artefacts arise from a worn X-ray anode and are ignored.

The lowermost spectrum (Fig. 5A) corresponds to a $SrTiO_3$(100) single crystal as received from the supplier. Contributions of strontium, titanium, oxygen and carbon can be detected. The small molybdenum contribution is due to the sample holder and it does not imply molybdenum content in the sample itself. No other elements are detected. The Fe content is well below the detection limit of the XPS setup used for the present investigation. A quantitative analysis using the areas under the Sr $3p_{3/2}$, Ti $2p_{3/2}$ and O 1s peaks indicates a stoichiometric strontium titanate contaminated by carbon, as can be seen from the presence of the C 1s peak.

To clean the sample, it was annealed in UHV at 700 °C for about two hours which was sufficient to remove the carbon contamination from the surface, as can be seen from spectrum B (Fig. 5). Also, it produced enough oxygen vacancies in the bulk to render the crystal conductible enough to be measured by MIES and UPS without charging. Otherwise, charging can pose a serious problem also for XPS. Spectrum A has been corrected by 5.5 eV charge-up to make comparison of the structures in B and C more convenient. For spectrum B no charging is observed. The surface of the $SrTiO_3$ remains the same because no change in $SrTiO_3$ stoichiometry compared to spectrum A can be detected.

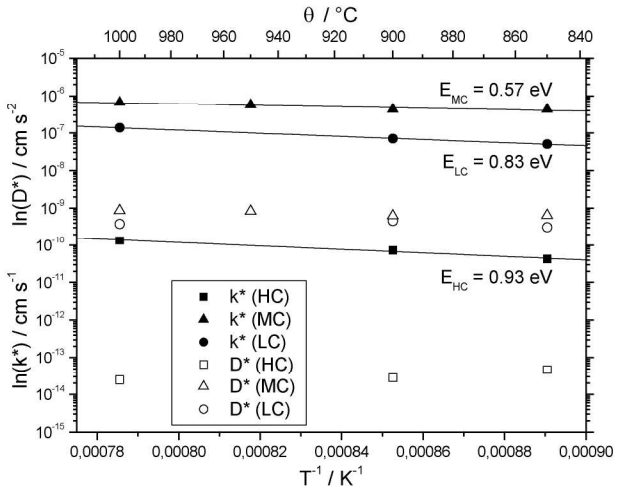

Fig. 4 Arrhenius plot for the ^{18}O surface exchange coefficients and diffusivities from $^{13}C^{18}O_2$ exposure.

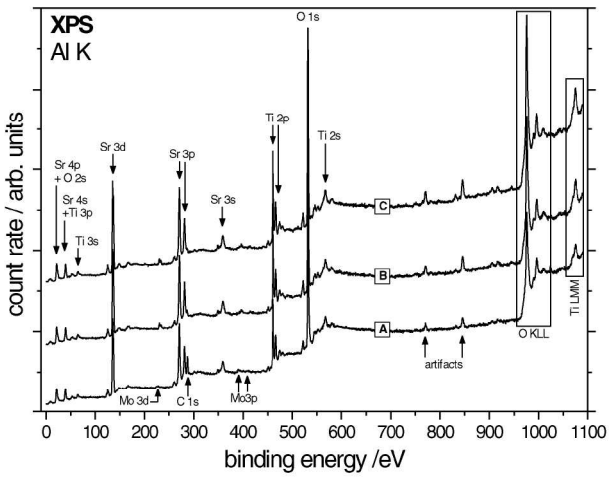

Fig. 5 XPS survey spectra of a $SrTiO_3$ (100) sample: (A) as received from the supplier, (B) annealed to 700 °C for two hours in UHV, (C) exposed to 600 L CO_2 at 500 °C.

For further experiments, the sample was stored under UHV conditions. Then, a short annealing to 500 °C was sufficient enough to restore the surface state in spectrum B.

In order to detect changes in the SDOS of the $SrTiO_3$, which can originate from adsorbates, an experiment where the $SrTiO_3$ surface was exposed to CO_2 under the permanent control of the MIES/UPS spectrometer has been performed. This can be seen in Fig. 6. The MIES and UPS spectra show the electron count rate plotted *versus* the electron binding energy with respect to the Fermi level at 0 eV in a waterfall manner. The progress of the experiment could be tracked on the right side with CO_2 exposure and annealing time indicated by arrows. Hence, the uppermost spectrum is the first and the lowermost spectrum the last one collected.

The experiment started with the surface being in state A, corresponding to the contaminated surface A as can be seen from Fig. 5. The surface exhibits a structured SDOS in MIES with two features at 10.6 eV and around 7 eV. The contributions beyond 10 eV are induced by secondary electrons and will not be discussed here. The SDOS is attributed to a carbon-containing contamination layer on the sample by comparison with preliminary experiments on $SrTiO_3$ and other surfaces. As can be observed from the development of the spectra, this contamination layer is easily removed from the surface by heating it up to 500 °C. The two features diminish and a single peak at 6.4 eV emerges (spectrum B, Fig. 5). A similar behaviour is observed in UPS, where two features at 7.1 eV and 4.9 eV develop during the heating procedure. These features are quite well known as the SDOS and near surface DOS of strontium titanate.[24] The peak at higher binding energy in UPS originates from the ionization of O 2p orbitals being hybridized with Ti 3d, while the peak at lower binding energy is due to nonhybridized O 2p states. These nonhybridized O 2p orbitals are present at the surface of the crystal, hence they are also detected in MIES as the single peak at 6.4 eV.

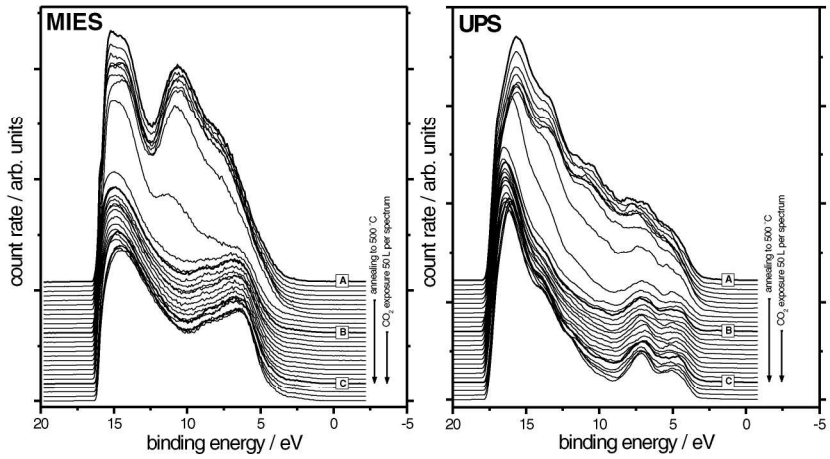

Fig. 6 MIES (left) and UPS (right) spectra of a CO_2 exposure experiment on a $SrTiO_3$(100) sample.

The presence of these features verifies that the crystal has the anticipated electronic structure and is titanium oxide terminated at state B.

Subsequently, the sample was kept at 500 °C and the surface was exposed to CO_2 at a rate of 50 Langmuir (L) per spectrum as indicated on the right side. Langmuir is a unit of exposure and equals 1.33×10^{-6} mbar s. The surface state is not changed by this treatment, as can be noticed from the unaltered MIES/UPS spectra (spectrum C, Fig. 5). Immediately after the CO_2 exposure, a XPS analysis was collected which is shown as spectrum C in Fig. 5. The analysis shows no change in the elemental composition of the crystal after CO_2 exposure. Furthermore, no carbon can be detected on the surface.

Additionally experiments (not shown here) were performed to clarify the gas exchange in front of the $SrTiO_3$ surface by means of a TPD system. For these experiments, the $SrTiO_3$ was heated to 1000 K in the presence of $^{13}C^{18}O_2$ and the change in gas composition directly in front of the sample was monitored as a function of $^{13}C^{18}O_2$ partial pressure. Once $^{13}C^{18}O_2$ is introduced into the recipient, $^{13}C^{18}O$ can be detected in front of the surface. The two partial pressures are linked by a linear relation. Other gases do not show such a relation.

4. Discussion

Oxygen is incorporated into $SrTiO_3$ by the dissociation of CO_2 into CO and O, probably through the following process:

$$CO_2(g) \Rightarrow CO(g) + O_{ads}^{-} + h^{\bullet} \quad (3)$$

$$O_{ads}^{-} + V_O^{\bullet\bullet} \Rightarrow O_O^{x} + h^{\bullet} \quad (4)$$

This means that during CO_2 dissociation two holes must be created in the STO surface. Because the investigated STO is acceptor doped, not enough surface electrons are available for a direct process under the experimental conditions. The sum reaction reads:

$$CO_2(g) + V_O^{\bullet\bullet} \Rightarrow CO(g) + O_O^{x} + 2h^{\bullet} \quad (5)$$

This model is backed up by our results: neither XPS nor MIES do show the presence of carbon on the surface of $SrTiO_3$ after the exposure of the crystal to CO_2. Furthermore, no contribution from the CO molecule is observed. Recent works on the CO dissociation at CaO surfaces[29] do show carbon remnants on the surface after the dissociation of CO, which are clearly identified by MIES and XPS. This means, that the CO resulting from the dissociation process is not further dissociated and is reemitted into the gas phase. This model is backed up by the TPD measurements, where the emission of CO from the $SrTiO_3$ surface could be observed directly.

Experiments at other temperature ranges (not shown here) yield similar results, even at room temperature. This means that the interaction with the CO_2 is a completely reversible process with no adsorbates remaining at the $SrTiO_3$ surface.

Nevertheless carbon monoxide ($^{13}C^{18}O$) can be involved in the oxygen exchange reaction[30] according to the reaction

$$C^{18}O(g) + {}^{16}O_O^{x} \Rightarrow C^{18}O^{16}O(g) + V_O^{\bullet\bullet} + 2e' \quad (6)$$

The electrons formed by reaction (6) can then be consumed for the direct incorporation

$$CO_2(g) + 2e' + V_O^{\bullet\bullet} \Rightarrow CO(g) + O_O^{x} \quad (7)$$

It is striking that both the k^* well as the D^* (Fig. 4) values are strongly dependent on dopant concentrations. It is expected that the higher the amount of Fe dopant the higher is the amount of oxygen vacancies, because of the Fe redox reaction

$$Fe_{Ti}^{x} \Leftrightarrow Fe_{Ti}' + h^{\bullet} \quad (8)$$

and the charge neutrality condition

$$[Fe_{Ti}'] + [e'] = 2[V_O^{\bullet\bullet}] + [h^{\bullet}] \quad (9)$$

with $[Fe_{Ti}'] = \text{const.}$ and $[e'] \approx 0$.

The higher the amount of oxygen vacancies the higher is the expected value of the diffusion coefficient. Also the surface exchange coefficient is expected to be higher with increasing dopant concentration because according to reaction (5) the vacancies are directly involved in the incorporation reaction.

However, this is not the case. Rather, they are 3 to 4 orders of magnitude lower in samples with high dopant concentration. This leads to the conclusion that higher concentrations of vacancies do not necessarily contribute to the oxygen diffusion. They seem rather to form associates and therefore the

jump probability for the oxygen ions is reduced, as described in the theory of the conservative ensembles[31] despite the high temperature in our experiments.

The activation enthalpy of the oxygen incorporation from the dissociation of a CO_2 source is rather low. As it can be seen in the Arrhenius plot in Fig. 4 they lie between 0.57 and 0.93 eV depending on the doping level.

5. Conclusions

Tracer diffusion coefficients and tracer surface oxygen exchange coefficients for the oxygen incorporation into Fe-doped $SrTiO_3$ from CO_2 dissociation are found to be strongly dependent on Fe concentrations. The diffusion coefficient increases with decreasing Fe concentration. CO_2 is believed to be dissociated into CO and oxygen. This oxygen incorporates into the material at high incorporation rates, practically comparable with the ones resulting from an oxygen atmosphere. The CO molecules are desorbed quite quickly. Further dissociation of CO into C and O is not conclusive from our study. Neither any trace of carbon is found on the surface of $SrTiO_3$ by examining the surface by means of XPS, MIES and UPS nor could any CO dissociation fragments be detected by TPD. The $SrTiO_3$ surface remains unchanged by the CO_2 exposure in terms of surface electronic structure and stoichiometry.

Acknowledgements

The financial support from the Deutsche Forschungsgemeinschaft (Contract no. Ma 1893/9 and Ar 248/3) for carrying out this work is gratefully acknowledged.

References

1 R. Moos, T. Bischoff, W. Menesklou and K. H. Härdtl, *J. Mat. Sci.*, 1997, **32**, 4247.
2 S. Steinsvik, R. Bugge, J. Gjønnes, J. Taftø and T. Norby, *J. Phys. Chem. Solids*, 1997, **58**, 969.
3 J. Padilla and D. Vanderbilt, *Surf. Sci.*, 1998, **418**, 64.
4 E. M. Logothetis, *Ceramic Engineering & Science Proceedings*, 1980, **1**, 281–301.
5 E. Ivers-Tiffée, K. H. Härdtl, W. Menesklou and J. Riegel, *Electrochim. Acta*, 2001, **47**, 807–814.
6 P. T. Moseley and D. E. Williams, *Polyhedron*, 1989, **8**, 1615–1618.
7 P. T. Moseley, *Sens. Actuators, B*, 1992, **6**, 149–156.
8 H. Meixner and U. Lampe, *Sens. Actuators, B*, 1996, **33**, 198–202.
9 J. Maier, in *Electrochemical Sensors*, ed. H. L. Tuller, J. Schoonman and I. Riess, Oxygen Ion and Mixed Conductors and their Technological Applications. Proceedings of the NATO Advanced Study Institute on Oxygen Ion and Mixed Conductors and their Technological Applications, Erice, Sicily, Italy, 15–30 July 1997. Dordrecht Boston London, (Kluwer Academic Publishers), 2000, pp. 399–421.
10 G. M. Choi and H. L. Tuller, *J. Am. Ceram. Soc.*, 1988, **71**, 201.
11 R. Moos and K. H. Härldtl, *J. Am. Ceram. Soc.*, 1997, **80**, 2549.
12 N. H. Chan, R. K. Sharma and D. M. Smyth, *J. Electrochem. Soc.*, 1981, **128**, 1762.
13 R. Merkle and J. Maier, *Angew. Chem., Int. Ed.*, 2008, **47**, 2.
14 W. Menesklou, H. J. Schreiner, K. H. Härdtl and E. Ivers-Tiffée, *Sens. Actuators, B*, 1999, **59**, 184.
15 R. Meyer and R. Waser, *Sens. Actuators, B*, 2004, **101**, 335.
16 K. Gömann, G. Borchardt, M. Schulz, A. Gömann, W. Maus-Friedrichs, B. Lesage, O. Kaïtasov, S. Hoffmann-Eifert and T. Schneller, *Phys. Chem. Chem. Phys.*, 2005, **7**, 2053.
17 J. Crank, *The Mathematics of Diffusion*, Clarendon Press, Oxford, 2nd edn, 1990.
18 M. Frerichs, F. Voigts and W. Maus-Friedrichs, *Appl. Surf. Sci.*, 2006, **253**, 950.
19 J. H. Scofield, *J. Electron Spectrosc. Relat. Phenom.*, 1976, **8**, 129.
20 C. J. Powell and A. Jablonski, *NIST Electron Inelastic-Mean-Free-Path Database - Version 1.1*, National Institute of Standards and Technology, Gaithersburg, MD, 2000, see http://www.nist.gov/srd/nist71.htm.
21 Y. Harada, S. Masuda and H. Ozaki, *Chem. Rev.*, 1997, **97**, 1897.
22 H. Morgner, *Adv. Atom. Mol. Opt. Phys.*, 2000, **42**, 387.
23 G. Ertl and J. Küppers, *Low Energy Electrons and Surface Chemistry*, VCH Verlag, Weinheim, 1985.
24 W. Maus-Friedrichs, M. Frerichs, A. Gunhold, S. Krischok, V. Kempter and G. Bihlmayer, *Surf. Sci.*, 2002, **515**, 499.
25 S. Bahr, A. Borodin, O. Höfft, V. Kempter and A. Allouche, *J. Chem. Phys.*, 2005, **122**, 234704.
26 J. Claus, M. Leonhardt and J. Maier, *J. Phys. Chem. Solids*, 2000, **61**, 1199.
27 Ch. Argirusis, S. F. Wagner, W. Menesklou, C. Warnke, T. Damjanović, G. Borchardt and E. Ivers-Tiffée, *Phys. Chem. Chem. Phys.*, 2005, **7**, 3523–3525.
28 S. F. Wagner, C. Warnke, W. Menesklou, Chr. Argirusis, T. Damjanović, G. Borchardt and E. Ivers-Tiffée, *Solid State Ionics*, 2006, **177**, 1607–1612.
29 F. Voigts, F. Bebensee, S. Dahle, K. Volgmann and W. Maus-Friedrichs, *Surf. Sci.*, 2009, **603**, 40.
30 C. A. Mims, N. Bayani, A. J. Jacobson and P. A. W. van der Heide, *Solid State Ionics*, 2005, **176**, 319.
31 J. Maier, *Physical Chemistry of Ionic Materials*, Wiley, Chichester, 2004.